Colloidal Synthesis of Organic-Capped ZnO Nanocrystals via a Sequential Reduction−Oxidation Reaction

P. Davide Cozzoli,*,[†] Andreas Kornowski, and Horst Weller

Institute of Physical Chemistry, University of Hamburg, Grindelallee 117-D20146 Hamburg, Germany

Received: September 21, 2004; In Final Form: November 24, 2004

A nonhydrolytic route to quantum-sized (d < 9 nm) ZnO nanocrystals in homogeneous organic solutions is presented. Nearly spherical ZnO nanocrystals were grown in a surfactant mixture of hexadecylamine and oleic acid (OLEA) by means of a two-step chemical process, based on the hot reduction (at 180−250 °C) of a zinc halide by superhydride ($LiBEt_3H$) followed by oxidation of the resulting product. The experimental results suggested that the controlled growth of ZnO in the nanosized regime depended both on the OLEA-assisted generation of intermediate metallic nanoparticles and on the adjustment of their oxidation conditions by using a mild oxidant, trimethylamine-*N*-oxide, rather than molecular oxygen. The present synthetic approach demonstrates to be particularly suitable to prepare organic-soluble ultra-small ZnO nanocrystals of low size dispersion and of stable size, which are appealing for optoelectronic, catalytic, and sensing purposes.

1. Introduction

Modern material chemistry attempts the design and the fabrication of nanostructured systems with tunable physical−chemical properties for advanced applications. Zinc oxide is one of the most attractive semiconductor oxides to be investigated at the nanoscale due to its promising applications in photovoltaic[1] and optoelectronic devices,[2,3] sensors,[4] varistors,[5] and (photo)catalysis.[6]

Despite the availability of a variety of wet-chemistry methods allowing the modulation of ZnO in various low-dimensional regimes[7] and intriguing morphologies,[8] the technological interest for extremely small (i.e., nearly spherical) nanocrystals still remains relevant.[1−6] As the decrease in the particle size actually scales with the increase in surface-to-volume ratio, a high interfacial transfer rate of photogenerated charge carriers, an elevated density of surface sites available for catalytic conversion,[6] and an efficient capture of solar light by the dye anchored on the particles in oxide-based dye-sensitized solar cells (DSCs)[1] are associated with a few nanometer-sized ZnO nanocrystals. Moreover, in such nanostructures, which show strong quantum-confinement effects, lasing may be facilitated because of the higher density of states near the band edges,[2−3a−d] provided that Auger recombinations effects do not dominate.[3e−g] Similarly, upon drastic reduction of the average grain size, the nominal voltage of varistors decreases while the response of gas sensors can be remarkably enhanced.[4−5]

The alkaline hydrolysis of zinc salts in alcoholic media at near room temperature has been the most widely applied solution-phase chemical route for the synthesis of ZnO nanocrystals owing to its simplicity, reproducibility, and low cost.[9] However, although some modifications[10] have been proposed to improve the original recipe, this method basically suffers for two main limitations. First, because of the absence of a strong repelling organic layer at their surface, the nanocrystals continue to grow slowly at low temperature via coarsening or epitaxial attachment,[11] even when capping ligands are introduced to quench growth.[12] As a consequence, such system inevitably evolves toward extensive particle aggregation and/or precipitation over several days. Second, as ZnO physical properties can be affected[13] by surface hydroxyl groups, adsorbed water, and/or precursor residuals deriving from the synthetic procedure, extreme thermal treatments are generally required to improve the stability and the reproducibility of material performances, however leading to sintering, grain growth, and loss of surface area in many cases.

In this scenario, the search for novel synthetic nonhydrolytic approaches mediated by the use of coordination chemistry could offer unexplored tools for achieving better control over the nanocrystal size and surface status, especially in the delicate case of ultra-small (3−5 nm) particles. Developments in the synthesis of II−VI semiconductor nanoparticles have established the potential of the thermal decomposition of organometallic precursors in coordinating solvents[14] to prepare high-quality metal oxide nanocrystals.[15] However, to date, just a few works have reported the successful application of this synthetic scheme to ZnO nanocrystals.[16] Recently, a room-temperature organometallic approach to size- and shape-controlled ZnO nanocrystals, which relies on the direct slow oxidation of a suitable zinc compound,[17] has been presented. An alternative strategy has also attracted interest, on the basis of the thermal oxidation of preformed zero-valent metal particles obtained upon decomposition of organometallic precursors under mild conditions. SnO_2,[18] In_2O_3,[19] CoO and Co_3O_4,[20] and ZnO[21] nanocrystals were derived by this method. Similarly, the combination of a sequential metal precursor decomposition−oxidation process with the use of hot surfactants has provided excellent results in terms of control over the particle size and size distribution in the case of γ-Fe_2O_3 nanocrystals.[22]

Following these latter findings, we have developed a novel nonhydrolytic route to quantum-sized (d < 8 nm) ZnO nanocrystals which consists of a two-step chemical process carried out in the same surfactant mixture of hexadecylamine (HDA) and oleic acid (OLEA): first, the hot (at 180−250 °C) reduction

---

* To whom correspondence should be addressed.
† Current address: Dipartimento di Chimica, Università di Bari, via Orabona 4-I-70126 Bari, Italy. Fax: +39 080 5442129. E-mail: d.cozzoli@ba.ipcf.cnr.it.

of a zinc halide by superhydride (LiBEt$_3$H), and second, reaction of the as-derived product with a mild oxidant, trimethylamine-*N*-oxide (TMAO). The obtained organic-capped ZnO nanocrystals were characterized by UV−vis absorption, photoluminescence (PL), Fourier-transform infrared (FTIR) spectroscopies, X-ray diffraction (XRD), and transmission electron microscopy (TEM). The experimental results suggested that the controlled growth of the ZnO in the nanosized regime depended both on the OLEA-assisted generation of intermediate metallic nanoparticles and on the adjustment of the oxidation conditions.

The present synthetic approach appears to be particularly suitable to prepare organic-soluble ultra-small ZnO nanocrystals of low size dispersion and of stable size, which are appealing for optoelectronic, catalytic, and sensing purposes.

2. Experimental Section

2.1. Chemicals. All chemicals were of the highest purity available and were used as received without further purification. Anhydrous zinc chloride (ZnCl$_2$, 99.999%), anhydrous zinc bromide (ZnBr$_2$, 99.999%), anhydrous trimethylamino-*N*-oxide ((CH$_3$)$_3$NO or TMAO, 98%), lithium triethylborohydride 1 M solution in THF (LiBEt$_3$H or "superhydride"), dioctyl ether ([CH$_3$(CH$_2$)$_7$]$_2$O or DOE, 99%), and oleic acid (C$_{18}$H$_{33}$CO$_2$H or OLEA, 90%) were purchased from Aldrich. *n*-Hexadecylamine (C$_{16}$H$_{33}$NH$_2$ or HDA, 90%) was purchased from Fluka.

All solvents used were of analytical grade and purchased from Aldrich.

2.2. Synthesis of ZnO Nanocrystals. *Two-Step Synthesis.* All manipulations were performed using standard air-free techniques unless otherwise stated. The reductant solution (2 M) was freshly prepared by mixing the 1 M superhydride solution in THF with previously degassed and N$_2$-saturated DOE and then by gently evaporating THF under vacuum. The resulting superhydride/DOE solution was kept at room temperature under nitrogen. In a typical synthesis, a mixture of HDA (10 g), a zinc salt (2 mmol), and OLEA (OLEA:ZnX$_2$ mole ratio was kept ≤ 1) was put into a 25-mL three-neck flask connected to reflux cooler and degassed for 1 h at 120 °C, after which the resulting clear solution was heated to high temperatures (in the range of 180−250 °C) under nitrogen flow. DOE (2 mL) reductant solution was loaded into a 5-mL syringe and then rapidly injected. Upon injection, the metal reduction occurred instantly, accompanied by a sudden change of the reaction mixture from colorless to black. Simultaneously, the temperature dropped to about 160−220 °C, and heating was maintained at these levels for the desired time period (referred to as "aging time", ranging from a few minutes to 1 h) to allow the metal clusters to grow further. Subsequently, the dark mixture was cooled to room temperature, and TMAO (6 mmol) was added under nitrogen flow. Oxidation of the suspended metallic product was then induced by slowly raising the temperature, recognized from the reaction mixture turning pale yellow in ∼3−15 min at 150−180 °C while remaining clear. Finally, the reaction was stopped by just removing the heat source and rapidly cooling the flask. The final ZnO nanocrystal size could be progressively increased from ∼3−9 nm by prolonging the aging time of the metal nanoparticles prior to their oxidation.

Alternatively, oxidation could be also carried out by gently bubbling an air flow by means of the tip of a stainless needle submerged in solution. In this case, the reaction occurred almost instantaneously at temperatures as low as ∼80−100 °C.

One-Step Synthesis. ZnO nanocrystals could be also obtained upon direct injection of a stoichiometric amount of the reductant solution into a mixture containing the surfactants, the metal precursor, and TMAO. This approach mainly yielded ∼3-nm nanocrystals. Bigger nanocrystals could be obtained by using the ∼3-nm nanoparticles as seeds in the presence of additional OLEA and ZnX$_2$. Dropwise (to suppress zinc nucleation in the bulk solution) addition of a calculated volume of superhydride solution was then carried out, followed by oxidation with TMAO, as described previously.

By application of both the one-step and the two-step syntheses, superhydride injection at temperatures lower than 150 °C did not allow us to finally obtain ZnO nanocrystals, as metal reduction did not occur or the metallic material initially formed tended to dissolve in a few seconds. Moreover, the direct mixing of ZnX$_2$ and TMAO without the introduction of superhydride did not yield ZnO nanocrystals. Prolonged heating at high temperatures exclusively led to TMAO decomposition, as inferred from the change of the reaction mixture from colorless to brownish.

Extraction Procedures. The extraction procedures were subsequently performed in air. The ZnO nanocrystals were readily precipitated upon addition of an excess of ethanol (or methanol) to the reaction mixture before amine solidification took place. The organic-capped ZnO nanocrystals could be separated from unwanted reaction byproducts by selective dissolution in chloroform, subsequent isolation by centrifugation from the insoluble precipitate (residual zinc salt precursor or eventual formed bulk zinc, depending on the reaction conditions), and renewed precipitation with methanol, followed by washing twice to remove TMAO and surfactant residuals. The OLEA-coated ZnO nanoparticles were then easily re-dispersed in solvents such as chloroform or hexane and stored over months without any further growth or irreversible precipitation.

The ZnO powders for XRD and FTIR analysis were prepared by washing the extracted precipitate repeatedly in order to remove physisorbed surfactant molecules and then evaporating the residual solvent under vacuum at room temperature.

2.3. Characterization Techniques. *UV−vis Absorption and Photoluminescence Spectroscopy.* Room-temperature absorption spectra were taken using a Cary 3 (Varian) spectrophotometer. An appropriate blank solution of HDA/OLEA in CHCl$_3$ was used as the reference. PL spectra of isolated ZnO nanoparticles in chloroform were measured at room temperature with a FluoroMax-2 spectrofluorimeter. Suitable filters to avoid second-order contributions were installed in the emission light path. PL spectra were measured of colloidal solutions having an optical density less than 0.3 at 280 nm to avoid reabsorption effects. PL spectra were normalized to the value of absorbance at the excitation wavelength.

Infrared Spectroscopy. FTIR spectra of ZnO powder were collected with a Bruker Equinox 55 spectrometer with a resolution of 4 cm^{-1}. Measurements were performed with pressed pellets, which were made using KBr powder as the diluent.

Powder XRD. XRD patterns of ZnO nanocrystal powders were collected with a Philips XPert diffractometer in Bragg−Brentano reflection geometry using filtered Cu Kα radiation (λ = 1.54056 Å). For XRD measurements, the nanocrystal powder was placed on a silicon sample holder.

TEM. Transmission electron microscopy (TEM) images were obtained using a Philips CM-300 microscope operating at 300 kV. The samples were prepared by dropping dilute solutions of isolated ZnO nanoparticles in chloroform onto 400-mesh carbon-coated copper grids and immediately evaporating the
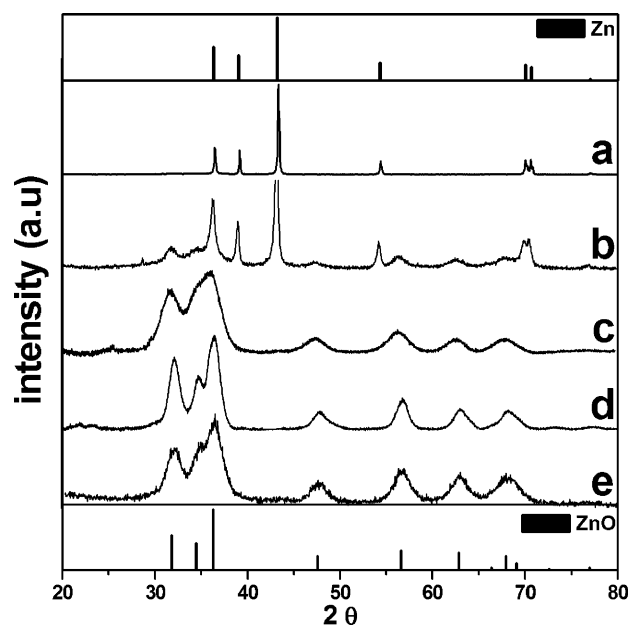
Figure 1. XRD pattern of the product obtained by the two-step (a−d) and by the one-step (e) methods. For all preparations 10 g of HDA, 2 mmol ZnBr2, 2 mL of 2 M superhydride, and 6 mmol TMAO were used; the injection was carried out at 200 °C and the oxidation step at 150 °C for 30 min. (a) Without OLEA; (b) 1 mmol OLEA; (c) 2 mmol OLEA, aging time 5 min; (d) 2 mmol OLEA, aging time 30 min; (e) 2 mmol OLEA, total growing time 30 min. The standard hexagonal Zn and wurtzite ZnO diffraction lines are also reported.

solvent. The samples were stable under the electron beam and did not degrade within the typical observation time.

3. Results

Two different procedures were applied to the synthesis of ZnO nanocrystals. In the first method, metal nanoparticles were initially formed upon zinc salt reduction by superhydride and were subsequently oxidized to zinc oxide in the native surfactant mixture. By this method, better control of particle size and size dispersion was reproducibly achieved in the range of 3−9 nm. In the second approach, the reductant was injected into the surfactant solution containing both the zinc salt precursor and the metal oxidant; the obtained $\sim$3-nm ZnO nanocrystals could be subsequently enlarged by a seed-mediated technique by adding more reactants. The obtained nanocrystals were characterized by TEM, XRD, UV−vis absorption and emission spectroscopy, and FTIR. In the following, the results of a typical synthesis under different experimental conditions are reported.

3.1. Structural and Morphological Characterization. Parts a−d of Figure 1 present the XRD pattern of the product obtained by reducing 2 mmol of $ZnBr_2$ in 10 g of HDA with a stoichiometric amount of superhydride/DOE solution at 200 °C followed by oxidation with TMAO (6 mmol) at 150 °C for 30 min.

In pure amine, the injection of the reductant resulted in the immediate formation of an insoluble black precipitate. Even after heating with added TMAO or O_2, the corresponding XRD pattern in Figure 1a matched well with that of bulk Zn metal (hexagonal phase).

Remarkable differences were found when OLEA was added as a cosurfactant in the growing mixture. At an OLEA:ZnX_2 mole ratio of $<\sim$0.8, the as-prepared samples were composed of a mixture of zinc and zinc oxide (Figure 1b); however, this latter appeared in nanosized crystalline domains, as inferred from the significant line broadening of the ZnO reflexes. In these

preparations, as the metallic product was nearly insoluble, ZnO could be separated by selective dissolution in apolar solvents, as described above. Interestingly, the XRD signals of Zn exhibited a progressive line-width broadening and intensity decrease with increasing the OLEA content, ascribable to a reduction of the metallic grain dimensions. At an OLEA:ZnX_2 mole ratio of $\sim$1, nanocrystalline domains of exclusive ZnO with increasing mean size could be obtained by simply prolonging the "aging time" of the reaction mixture before the oxidation step while the product remained well-dissolved into the growing mixture at all stages during preparation. For example, the narrowing in the ZnO diffraction peaks with increasing "aging time" from 5 to 30 min (in parts c and d of Figure 1, respectively) correlated well with the increase in the average nanocrystal size from 3.2 to 6.9 nm, as estimated using the Debye−Scherrer formula.

Finally, at OLEA:ZnX_2 > 1.5, no precipitate could be collected as the initially formed metal product underwent dissolution.

As a further example, in Figure 1e, the XRD pattern of the material obtained by applying the one-step synthetic method is shown. The injection of superhydride into a HDA/OLEA/TMAO/ZnX_2 mixture yielded $\sim$3-nm nanosized crystalline domains of pure ZnO.

The morphology of the material and its crystallographic structure were revealed by TEM measurements. In absence of OLEA, Zn nanocrystals grew uncontrollably with the sample morphology mainly being characterized by tightly agglomerated particles, having irregular shapes and very large sizes (>100 nm). In Figure 2 the typical bright-field (BF) images of various ZnO samples grown in the presence of OLEA are reported. In the case of the product obtained by employing TMAO as the oxidant (parts a−d of Figure 2), the samples apparently consisted of well-separated single nanoparticles, showing no tendency to aggregate because of their organic surface capping. The crystallinity of the nanoparticles was confirmed by HRTEM studies (data not shown). Nearly spherical ZnO nanocrystals of narrow size distribution could be actually prepared by applying the two-step method. For example, the mean particle size could be modulated between $\sim$3 and $\sim$7 nm (parts a and b of Figure 2) simply by increasing the aging time preceding the forced oxidation step with the particle value measured by TEM being in good agreement with that calculated from the XRD pattern (parts c and d of Figure 1, respectively). Figure 2c illustrates that uniformly sized spherical ZnO nanocrystals could be directly obtained by injecting the reductant into a HDA/OLEA/ZnX_2/TMAO mixture by the one-step method. A change in both size and morphology was detected upon carrying out an enlargement procedure that used the as-prepared $\sim$3-nm particles as the initial seeds to be grown further (Figure 2d). In fact, the resulting nanocrystals, although retaining their individuality, had a broader size dispersion (centered at $\sim$8 nm) and also a moderate shape distribution, including ellipsoidal, rodlike, and polycrystalline particles.

As an additional example, Figure 2e reports a TEM image of nanocrystals that were prepared under the same conditions as for the sample in Figure 2b except for the fact that the oxidation step was conducted by using an air flow. Interestingly, the ZnO nanocrystals obtained via this route were characterized by a significantly broader size distribution and a high degree of agglomeration that prevented the accurate inspection of their morphology. Such nanoparticle features were observed in all preparations in which O_2 acted as the oxidant, irrespective of the mean particle size.
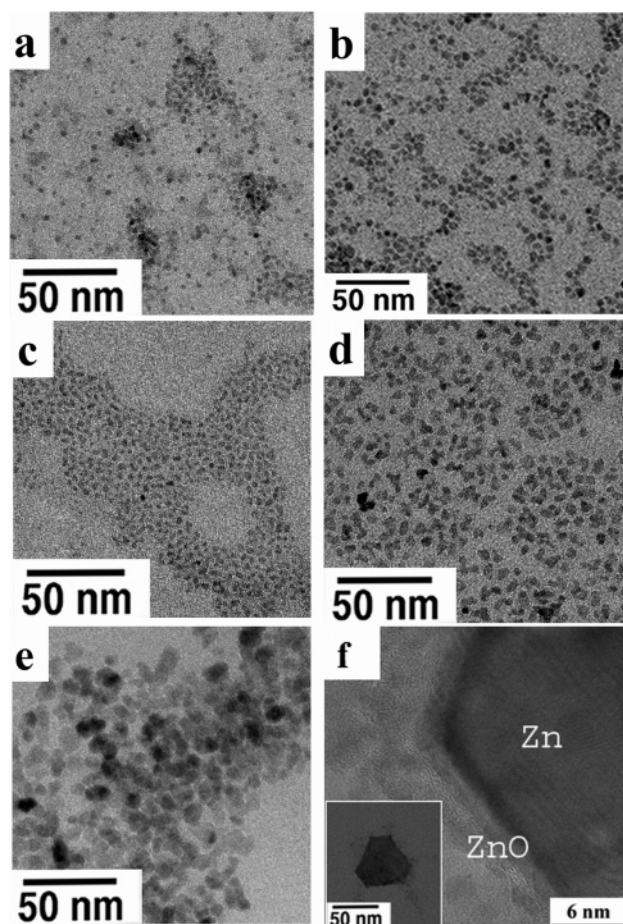
Organic-Capped ZnO Nanocrystals

J. Phys. Chem. B, Vol. 109, No. 7, 2005 **2641**

Figure 2. TEM overview of ZnO nanocrystals prepared in 10 g of HDA, 2 mmol OLEA, 2 mmol ZnBr2, 2 mL of 2 M superhydride injected at 200 °C. (a and b) Two-step method, oxidation period 30 min at 150 °C with 5 and 30 min aging times, respectively. (c and d) One-step method, as-prepared and after seeded growth, respectively. (e) Same conditions as sample b but using O_2 as the oxidant. (e) HRTEM of a faceted Zn particle with oxidized surface.

Because of their remarkable sensitivity to air, Zn nanoparticles of a few nanometers (the black material dissolved formed upon reductant injection), which were supposed to act as precursors for the ZnO nanocrystals, could not be isolated for a time sufficient for structural characterization. However, in samples prepared at an OLEA:ZnX_2 mole ratio smaller than 1, both spherical ZnO nanocrystals and widely polydisperse (20−200 nm) Zn crystals could be observed. When not agglomerated, the latter resulted in being soluble in apolar media like the oxide nanoparticles and could be thus imaged in detail by TEM. In most cases, such zinc nanoparticles appeared faceted. Figure 2f shows a representative example. The HRTEM image clearly reveals that the nanoparticle is characterized by a different image contrast at the surface region. By measurement of the respective lattice distances, it could be inferred that the metal nanoparticle was actually composed of a Zn core surrounded by a coherently grown ZnO crystalline shell.

3.2. Optical Characterization. Samples prepared in the presence of OLEA provided optically clear nonpolar solutions after extraction from the growing medium. In Figure 3, the absorption spectra and the PL emission spectra of two selected ZnO samples of different size, namely ∼3 nm (Figure 3a) and ∼7 nm (Figure 3b), are reported.

A significant blue-shift of the band-edge absorption with respect to the bulk material (373 nm) was measured (Figure 3, left axis). In addition, the first exciton feature narrowed and
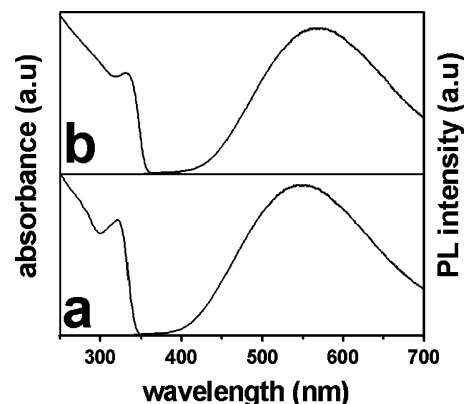

Figure 3. Absorption (left axis) and corresponding normalized room-temperature PL emission (right axis, $\lambda_{ex} = 300$ nm) spectra for two ZnO selected samples of ∼3 nm (a) and ∼7 nm (b) in CHCl₃. In part a, the PL emission spectrum is scaled by a factor of 5.
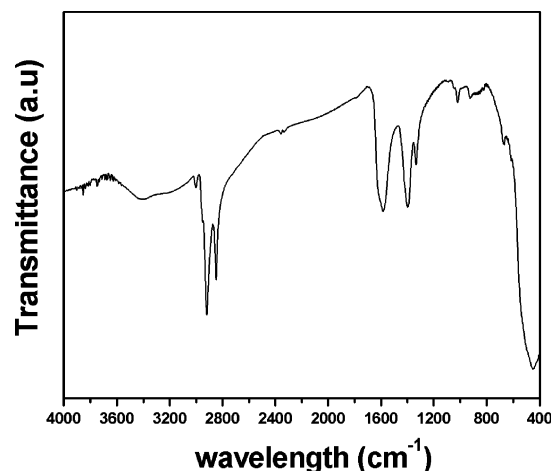

Figure 4. Typical FTIR spectra in the 4000−400-cm⁻¹ region of the as-prepared organic-capped ZnO nanocrystals.

became better resolved with decreasing particle size. Such optical features implied that the nanocrystals were in a strongly quantum-confined dimensional regime.[9] The absorption spectra of ZnO nanocrystals prepared by the seeded growth technique did not exhibit relevant differences at constant mean particle size, except for a broadening of the exciton absorption peak. As general behavior, the PL emission (Figure 3, right axis) of the nanocrystals consisted of a broad intense green band, irrespective of the nanocrystal size, attributed to trap-state exciton recombination.[23] No detectable UV band, ascribable to band-edge recombination, could be detected in anhydrous and oxygen-free solution, even upon UV irradiation.[9]

Notably, the colloidal stability of the ZnO nanocrystal organic solution remained unchanged at room temperature for several weeks after preparation under ambient atmosphere, as neither material precipitation nor significant absorption changes could be detected. Also, their emission properties remained unchanged over the same time period.

3.3. Surface Properties. The nature of the organic coating on the surface of the ZnO nanocrystals was investigated by FTIR spectroscopy and interpreted on the basis of previously reported studies on the anchoring of organic ligands onto the surface of oxides.[13a−b,17b, 24]

In Figure 4, the typical IR spectra of a ZnO nanocrystal sample is shown in the 4000−400-cm⁻¹ region. Above 2000 cm⁻¹, the intense antisymmetric and symmetric C−H stretching vibrations[24] (at 2920 and 2850 cm⁻¹, respectively) of the

−CH$_2$− groups in the hydrocarbon moiety were observed. The shoulder at 2960 cm^{-1} could be associated with the asymmetric stretching of the terminal −CH$_3$ group of the alkyl chain. Notably, a weak but definite band was also distinguishable at 3008 cm^{-1}, ascribable to the olefinic C−H stretching.[24b] In addition, the C−H stretching signals were superimposed on an underlying surface O−H broad stretching band centered at ~3300 cm^{-1}. Below 2000 cm^{-1}, the antisymmetric and symmetric stretching vibrations (two characteristic bands centered at 1582 and 1403 cm^{-1}, respectively) of carboxylate groups[13a−b] complexed with surface Zn centers dominated in the spectra of the nanocrystals. As the value of their frequency difference ($\Delta\nu \approx 179$ cm^{-1}) is considerably higher than that in the corresponding ionic salt ($\Delta\nu \approx 94$ cm^{-1} for zinc acetate), the mode of binding of carboxylate adsorbates onto the ZnO surface might be interpreted as being unidentate[13a−b,24b,24d] although the broadness of the bands and the presence of an additional peak at 1334 cm^{-1} cannot exclude the presence of other carboxylate complexed structures.

Moreover, the expected weak contributions from the −CH$_2$− bending (at ~1450−1470 and ~1330 for the antisymmetric and symmetric modes, respectively), the C−O−H bending (~1410 cm^{-1}), the C−OH stretching (~1280 cm^{-1}), the N−H bending (~1580 cm^{-1}), and the C−N bending (at 1316 cm^{-1} in HDA)[17b] bands cannot be unambiguously discerned, owing to the coincidence of many signals in the same spectral region. Below 600 cm^{-1}, the characteristic stretching of Zn−O bonds in zinc oxide is observable.

4. Discussion

In this report, a novel chemical route to ZnO nanocrystals in homogeneous organic solutions has been presented. ZnO nanocrystals were grown in surfactant mixtures by means of a sequential reduction−oxidation process, aiming for the generation of nanometer-sized metal nanoparticles by hot reduction of a zinc salt with superhydride, followed by their oxidation with a mild oxidant, TMAO. The results shown here demonstrate that the present route yielded quantum-sized ZnO nanocrystals (3−8 nm) when OLEA was used in combination with HDA. The average particle size could be easily tuned by simply changing a few reaction parameters. The possibility of achieving a control over both the reduction and the oxidation step allowed the facile synthesis of organic-capped, nonaggregated nanocrystals, easily redispersible in organic solvents.

The synthesis of nanosized metal zinc has been rather rarely reported in the literature.[21,25] Difficulties in the preparation of zinc nanoparticles are intrinsically related to their high susceptibility to oxidation owing to their favorable inherent redox potential, which is progressively shifted to even more negative values than the conventional bulk electrode value with decreasing the particle size.[26] The pronounced sensitivity of zinc nanoparticles toward trace amounts of oxygen and moisture actually prevents them from being isolated by means of conventional solvent/nonsolvent extraction procedures, unless all processing and even sampling for characterization of the material are carried out under rigorously inert atmosphere.[21]

On the basis of this chemical reactivity, a strategy was therefore employed aiming for the formation of zinc clusters that could act as highly reactive intermediates for the production of their oxidized counterparts under controlled conditions. Subsequent in situ introduction of an oxidant actually led to conversion of the metal nanoparticles to zinc oxide nanocrystals.

The collected data showed that two conditions should be fulfilled in order to obtain well-dispersed pure zinc oxide nanocrystals of narrow size-distribution: first, the parent metal clusters should be obtained relatively monodisperse in the nanometer-sized range in order to automatically restrict[18−22] the dimensional regime and the size distribution of the derived ZnO nanocrystals (a mass increase was obviously expected to accompany the full oxidation of the metal nanoparticles); second, the rate of oxidation should be slow enough to preserve the nanoparticles against undesired coalescence or aggregation during their conversion into the oxide. Both issues are discussed as follows.

Solution phase metal salt reduction under inert atmosphere is a well-known technique for the preparation of metal nanoparticles under the assistance of a variety of organic ligands.[27] It is broadly accepted that a temporal separation of the nucleation and growth stages is desirable for the production of a monodisperse colloid. Ideally, a large number of critical nuclei should be formed in a short interval of time followed by the simultaneous and steady growth of those nuclei. In the proposed synthetic approach, a strong reducing agent, superhydride,[27a] was injected to induce the rapid reduction of Zn(II) halide in hot (180−250 °C) media. This procedure provided the temporally discrete homogeneous nucleation desired. Growth of the nuclei was continued by addition of zinc-containing species to the surface of the nanoparticles and could be halted by cooling to room temperature.

A mixture of surfactants, alkylamines and oleic acid, was employed to control growth of the nanoparticles and protect them from aggregation. Following the initial nucleation event, the increase in metal size was likely sustained via a seed-catalyzed growth mechanism.[28] Alkylamine would reversibly coordinate neutral metal surface sites, slowing but not stopping the particle's growth. This is in agreement with the observation that this surfactant alone could not, in fact, prevent the zinc clusters from eventually enlarging to undispersible aggregates or bulk material. Oleic acid is an excellent stabilizing agent; however, it binds so tightly to the particle surface during synthesis that it could redissolve the zinc clusters initially formed or even inhibit nucleation when employed at high concentration and/or at lower temperatures (<150 °C). As opposed, the combination of alkylamine/oleic acid within a suitable range for the OLEA:Zn mole ratio produced a tight ligand shell that allowed the particles to grow steadily while preserving them against uncontrolled coalescence.

As a matter of fact, the adjustment of OLEA/Zn precursor mole ratio in the growing mixture was essential to guarantee the generation of colloidally stable nanometer-sized metal nanoparticles as suitable precursors for fully oxidized nanocrystals. In the absence of OLEA, injection of the reductant solution resulted in the immediate precipitation of bulk zinc in the hot vessel. At low OLEA concentration (OLEA/ZnX$_2$ mole ratio < ~0.8), both large Zn crystals and ZnO nanocrystals were ultimately obtained, the nanoparticle yield being approximately proportional to the OLEA content. In addition, at too-high OLEA content (OLEA/ ZnX$_2$ mole ratio > ~1.5), only the transient darkening of the reaction mixture was observed, indicative for initial metal reduction and subsequent dissolution of unstable clusters. This experimental evidence is reasonably in agreement with the formation of a Zn(II):OLEA complex, which would help in regulating the supply of Zn monomer species for metal cluster growth. An OLEA:Zn mole ratio of ~1 was found optimal to allow for a constant particle growth in the nanometer-sized regime.

Although the parent Zn nanoparticles could not be isolated and imaged by TEM, their presence as reactive intermediates

Organic-Capped ZnO Nanocrystals

J. Phys. Chem. B, Vol. 109, No. 7, 2005 **2643**

was suggested by two main observations. First, the direct mixing of the ZnX_2 with TMAO or O_2 yielded no ZnO, thus indicating that the Zn(II):OLEA complex in solution did not react with the oxidant. Second, under conditions (i.e., at low reduction temperatures and/or at high OLEA content) which inhibited metal nucleation or growth, no crystalline material was finally obtained. This was obviously because only the Zn(II):OLEA complex again remained in the growing mixture. Both pieces of evidence allowed the postulate that TMAO or O_2 should actually attack Zn(0) nanoparticles and then convert them to ZnO. Therefore, it could be concluded that the introduction of superhydride at high temperature was required to nucleate and steadily grow the sacrificial metallic nanoparticles. Accordingly, it could be reasonably presumed that the zinc nanocrystal size increased with prolonging the aging time, as the resulting ZnO nanocrystals were progressively bigger. By the same argument, the morphology of the nanoparticles could be expected to be conserved throughout the oxidation process, as previously found for many other materials.[18-22] An exception seemed to be represented by the nanoparticles grown by the seed-mediated technique, which showed a variety of anisotropic shapes. This fact may be explained by invoking an initial asymmetric[29,30b] nucleation of a Zn shell onto a ZnO seed during the dropwise reductant addition, possibly due to a differential reactivity among the various crystal facets, and eventually promoted by the face-selective surfactant adsorption.

As clearly seen in the two-step method, the modality of the oxidation step affected the aggregation status of the resulting oxide material significantly. In relatively large metal particles or bulk material, mild oxidation only led to surface passivation which appeared as means of considerably reducing the rate of further oxidation.[21,30b] The complete conversion of such exceedingly giant metal particles into the corresponding oxide can be reasonably expected to require more drastic reaction conditions than those adopted in the present procedure,[30] which were thus applied successfully only to a few nanometer-sized metal particles. Accordingly, our controlled experiments concluded that the generation of ZnO nanocrystals could directly occur via progressive oxidation of nearly bulk Zn crystals as sacrificial substrate.

Although the crystallinity of the oxide nanoparticles was elevated in all cases, well-separated nanocrystals were obtained only if TMAO was the oxidant, whereas aggregation was seen with the use of air flow. It is conceivable that such differences have to be related to the faster oxidation rate induced by molecular oxygen, as observed experimentally.

In the mechanism of seed-catalyzed metal particle growth, the initially formed metal nuclei can accelerate further metal ion reduction by mediating electron transfer from the reductant to the ions in solution. Charge injection on metallic particles displaces their redox potential to even more negative potentials than in uncharged particles, thus rendering them very susceptible to oxidation. As expected from its ability in efficiently scavenging electrons, O_2 would violently attack the metal clusters, causing their surface atoms to rearrange and the related ligand shell to lose its coordination properties. This could, in turn, facilitate particle coalescence, therefore explaining the observed tendency of the formed ZnO nanocrystals to aggregate. As opposed, metal reaction with TMAO[15e,22] should be sufficiently slow to simultaneously allow the surfactant restructuring on the surface of the just-formed oxide as well as perfect core crystallization.

Although HDA was important in mediating growth, FTIR analysis indicated that only the more strongly binding ligand,

OLEA, remained coordinated to the nanocrystal surface when isolated from the growth solution. Although the unique assignment of the binding structure of the carboxylate ligands on the surface was difficult, the nature of ZnO surface passivation undoubtedly accounted for both the colloidal stability and the unchanged luminescence intensity of ZnO nanoparticles for a long period after preparation at room temperature in air atmosphere.

In our samples, the UV emission (due to band-edge recombination) was not observed. The dominance of the UV emission in PL spectra has been rarely observed for ZnO nanocrystals, except for organic-passivated nanoparticles[31,32] or upon UV irradiation in deaerated alcoholic media.[9,23] Oxygen vacancies have been recognized to be involved in the visible luminescence of ZnO, attributed to a recombination[23] of a photogenerated electron from the conduction band edge (or from a shallow level close to the conduction band edge) to a deeply trapped hole in the bulk. As the ZnO nanocrystals were grown in anhydrous and oxygen-free solvents, they could be expected to be oxygen deficient,[16] with the oxygen vacancies mainly located on the surface. In our data, the size dependence of the emission can also be explained on the basis of an efficient surface hole trapping at an O^{2-} site.[32] The luminescence intensity might be possibly related to unidentate carboxylate complexes on the oxide surface, as such structures have been assumed[13a-b] to efficiently trap the photogenerated holes through the electron-richer carbonyl group as compared to other complexes.

5. Conclusions

A nonhydrolytic route to organic-soluble ZnO nanocrystals in homogeneous solutions has been presented. Handy chemicals have been easily manipulated in two-step reduction−oxidation reactions under the coordinating action of suitable surfactants. The present synthesis can be scaled up for the preparation of colloidally stable luminescent ZnO nanocrystals of low size dispersion and of any desired size in the quantum-sized regime.

The proposed sequential scheme can be potentially extended to the preparation of other materials (for instance InAs, InP, and so on) for which the decomposition of toxic and unstable organometallic precursors is so far the most commonly applied approach. In this regard, the inclusion of a reduction step of a suitable metal salt in the synthetic procedure may be expected to pave the way to more versatile and "greener" synthetic routes for other technologically relevant semiconductor nanocrystals.

References and Notes

(1) (a) Rensmo, H.; Keis, K.; Lindstrom, H.; Solbrand, A.; Hagfeldt, A.; Lindquist, S. E.; Wang, L. N.; Muhammed, M. *J. Phys. Chem. B* **1997**, *101*, 2598. (b) Bauer, C.; Boschloo, G.; Mukhtar, E.; Hagfeldt, A. *J. Phys. Chem. B* **2001**, *105*, 5585.

(2) (a) Tennakone, K.; Kamura, G. R.; Kottegoda, I. R.; Perera, V. P. *Chem. Commun.* **1999**, 15. (b) Zhang, X. T.; Liu, L. G.; Zhang, L. G.; Zhang, Y. M.; Lu, M.; Shen, Z.; Xu, W.; Zhong, G. Z.; Fan, X. W.; Kong, X. G. *J. Appl. Phys.* **2002**, *92*, 3293. (c) Johnson, J. C.; Yan, H.; Schaller, R. D.; Haber, L. H.; Saykally, R. J., Yang, P. *J. Phys. Chem. B* **2001**, *105*, 11387.

(3) (a) Govender, K.; Boyle, D. S.; O'Brien, P.; Binks, D.; West, D.; Coleman, D. *Adv. Mater.* **2002**, *14*, 1221. (b) Yoshida, T.; Minomura, H. *Adv. Mater.* **2000**, *12*, 1219. (c) Yoshida, T.; Terada, K.; Schlettwein, D.; Oekermann, T.; Suiura, T.; Minomura, H. *Adv. Mater.* **2000**, *12*, 1214. (d) Huang, M. H.; Mao, S.; Feick, H.; Yan, H.; Wu, Y.; Kind, H.; Weber, R.; Russo, R.; Yang, P. S. *Science* **2001**, *292*, 1987. (e) Klimov, V. I.; Mikhailovski, A. A.; McBranch, D. W.; Leatherdale, C. A.; Bawendi, M. G. *Science* **2000**, *287*, 1011. (f) Kharchenko, V. A.; Rosen, M. *J. Lumin.* **1996**, *70*, 158. (g) Klimov, V. I.; Mikhailovski, A. A.; Xu, S.; Malko, A.; Hollingsworth, J. A.; Leatherdale, C. A.; Eisler, H.-J.; Bawendi, M. G. *Science* **2000**, *290*, 314.

(4) (a) Dong, L. F.; Cui, Z. L.; Zhang, Z. K. *Nanostruct. Mater.* **1997**, *8*, 815. (b) Chadwick, A. V.; Russell, N. V.; Whitham, A. R.; Wilson, A. *Sens. Actuators, B* **1994**, *18−19*, 99.

(5) (a) Gupta, T. K. *J. Am. Ceram. Soc.* **1990**, *73*, 1817. (b) Hennings, D. F. K.; Hartung, R.; Reijnrn, P. J. *J. Am. Ceram. Soc.* **1990**, *73*, 645. (c) Raghu, N.; Kutty, T. R. *Appl. Phys. Lett.* **1992**, *60*, 100.

(6) (a) Ramakrishna, G.; Ghosh, H. N. *Langmuir* **2003**, *19*, 3006. (b) Kamat, P. V.; Huehn, R.; Nicolaescu, R. *J. Phys. Chem. B* **2002**, *106*, 788. (c) Curri, M. L.; Comparelli, R.; Cozzoli, P. D.; Mascolo, G.; Agostiano, A. *Mater. Sci. Eng. C* **2003**, *23*, 285. (d) Marci, G.; Augugliaro, V.; Lopez-Munoz, M.; Martin, C.; Palmisano, L.; Rives, V.; Schiavello, M.; Tilley, R. J. D.; Venezia, A. M. *J. Phys. Chem. B* **2001**, *105*, 1026. (e) Marci, G.; Augugliaro, V.; Lopez-Munoz, M.; Martin, C.; Palmisano, L.; Rives, V.; Schiavello, M.; Tilley, R. J. D.; Venezia, A. M. *J. Phys. Chem. B* **2001**, *105*, 1033.

(7) (a) Taubert, A.; Palms, D.; Weiss, O.; Piccini, M.; Batchelder, D. N. *Chem. Mater.* **2002**, *14*, 2594. (b) Taubert, A.; Glasser, G.; Palms, D. *Langmuir* **2002**, *18*, 4488. (c) Guo, L.; Yang, S.; Yang, C.; Yu, P., Wang, J.; Ge, W.; Wong, K. L. *Chem. Mater.* **2000**, *12*, 2268. (d) Kaneko, D.; Shouji, H.; Kawai, T.; Kon-No, K. *Langmuir* **2000**, *16*, 4086.

(8) (a) Pacholski, C.; Kornowski, A.; Weller, H. *Angew. Chem., Int. Ed. Engl.* **2002**, *41*, 7, 1188. (b) Vayssieres, L. *Adv. Mater.* **2003**, *15*, 464. (c) Liu, B.; Yu, S.-H.; Zhang, F.; Li, L.; Zhang, Q.; Ren, L.; Jiang, K. *J. Phys. Chem. B* **2004**, *108*, 4338. (d) Wang, Z.; Qian, X.-f.; Yin, J.; Zhu, Z.-K. *Langmuir* **2004**, *20*, 3441. (e) Ji, Y. L.; Guo, L.; Xu, H.; Simon, P.; Wu, Z. *J. Am. Chem. Soc.* **2002**, *124*, 14864. (f) Liu, B.; Zeng, H. C. *J. Am. Chem. Soc.* **2003**, *125*, 4430.

(9) (a) Bahnemann, D.; Kormann, C.; Hoffmann, M. R. *J. Phys. Chem.* **1987**, *91*, 3789 (b) Spanhel, L.; Anderson, M. A. *J. Am. Chem. Soc.* **1991**, *113*, 3, 2826.

(10) (a) Wong, E.; Bonevich, J. E.; Searson, P. C. *J. Phys. Chem. B* **1998**, *102*, 7770. (b) Meulenkamp, E. A. *J. Phys. Chem. B* **1998**, *102*, 5566. (c) Tokumoto, M. S.; Pulcinelli, S. H.; Santilli, C. V.; Briosi, V. *J. Phys. Chem. B* **2003**, *107*, 568. (c) Rodroguez-Gattorno, G.; Santiago Jacinto, P.; Rendon-Vazquez, L.; Nemeth, J.; Dekany, I.; Diaz, D. *J. Phys. Chem. B* **2003**, *107*, 12597.

(11) (a) Oskam, G.; Hu, Z.; Penn, R. L.; Pesika, N.; Searson, P. C. *Phys. Rev.* **2002**, *E66*, 114031. (b) Hu, Z.; Oskam, G.; Penn, R. L.; Pesika, N.; Searson, P. C. *J. Phys. Chem. B* **2003**, *107*, 3124.

(12) (a) Wong, E. M.; Hoertz, P. G.; Liang, C. J.; Shi, B.; Meyer, G. J.; Searson, P. C. *Langmuir* **2001**, *17*, 8362. (b) Pesika, N. S.; Hu, Z.; Stebe, K. J.; Searson, P. C. *J. Phys. Chem. B* **2002**, *106*, 6985.

(13) (a) Sakohara, S.; Tickanen, L. D.; Anderson, M. A. *J. Phys. Chem.* **1992**, *96*, 11086. (b) Sakohara, S.; Ishida, M.; Anderson, M. A. *J. Phys. Chem. B* **1998**, *102*, 10169−10175. (c) Monticone, S.; Tufeu, R.; Kanaev, A. V. *J. Phys. Chem. B* **1998**, *102*, 2854.

(14) Murray, C. B.; Norris, D. J.; Bawendi, M. G. *J. Am. Chem. Soc.* **1993**, *115*, 8706.

(15) (a) Rockenberger, J.; Scher, E. C.; Alivisatos, A. P. *J. Am. Chem. Soc.* **1999**, *121*, 11595. (b) Trentler, T. J.; Denler, T. E.; Bertone, J. F.; Agrawal, A.; Colvin, V. L. *J. Am. Chem. Soc.* **1999**, *121*, 1613. (c) Niederberger, M.; Bartl, M. H.; Stucky, G. *Chem. Mater.* **2002**, *14*, 4364. (d) Niederberger, M.; Bartl, M. H.; Stucky, G. D. *J. Am. Chem. Soc.* **2002**, *124*, 13642. (e) Yin, M.; O'Brien, S. *J. Am. Chem. Soc.* **2003**, *125*, 10180.

(16) (a) Shim, M.; Guyot-Sionnest, P. *J. Am. Chem. Soc.* **2001**, *123*, 11651. (b) Cozzoli, P. D.; Curri, M. L.; Agostiano, A.; Leo, G.; Lomascolo, M. *J. Phys. Chem. B* **2003**, *107*, 4756.

(17) Monge, M.; Kahn, M. L.; Maisonnat, A.; Chaudret, B. *Angew. Chem., Int. Ed. Engl.* **2003**, *115*, 5749.

(18) Nayral, C.; Ould-Ely, T.; Maisonnat, A.; Chaudret, B.; Fau, P.; Lescouzeres, L.; Peyre-Lavigne, A. *Adv. Mater.* **1999**, *11*, 61. (b) Nayral, C.; Viala, E.; Fau, P.; Senocq, F.; Jumas, J. C.; Maisonnat, A.; Chaudret, B. *Chem.−Eur. J.* **2000**, *6*, 4082.

(19) Soulantica, C.; Erades, L.; Sauvan, M.; Senocq, F.; Maisonnat, A.; Chaudret, B. *Adv. Funct. Mater.* **2003**, *13*, 553.

(20) Verelst, M.; Ely, T. O.; Amiens, C.; Snoeck, E.; Lecante, P.; Mosset, A.; Respaud, M.; Broto, J. M.; Chaudret, B. *Chem. Mater.* **1999**, *11*, 2702.

(21) Rataboul, F.; Nayral, C.; Casanove, M. J.; Maisonnat, A.; Chaudret, B. *J. Organomet. Chem.* **2002**, *643−644*, 307.

(22) Hyeon, T.; Lee, S. S.; Park, J.; Chung, Y.; Na, H. B. *J. Am. Chem. Soc.* **2001**, *123*, 12798.

(23) (a) Van Dijken, A.; Janssen, A. H.; Smitsmans, M. H. P.; Vanmaekelbergh, D.; Meijerink, A. *Chem. Mater.* **1998**, *10*, 3513. (b) Van Dijken, A.; Meulenkamp, E. A.; Vanmaekelbergh, D.; Meijerink, A. *J. Phys. Chem. B* **2000**, *104*, 1715.

(24) (a) Hesse, M.; Meier, H.; Zeeh, B. *Spektroskopisce Methods in der Organiscen Chemie*; George Thieme Verlag: Stuttgart, New York. (b) Thistlethwaite, P. J.; Hook, M. S. *Langmuir* **2000**, *16*, 4993. (c) Nara, M.; Torii, H.; Tasumi, M. *J. Phys. Chem.* **1996**, *100*, 19812. (c) Thistlethwaite, P. J.; Gee, M. L.; Wilson, D. *Langmuir* **1996**, *12*, 6487. (d) Nara, M.; Torii, H.; Tasumi, M. *J. Phys. Chem.* **1996**, *100*, 19812.

(25) (a) Kimura, K.; Bandow, S. *J. Colloid Interface Sci.* **1995**, *171*, 356. (b) Kimura, K. *J. Colloid Interface Sci.* **1996**, *183*, 607.

(26) (a) Henglein, A. *Chem. Rev.* **1989**, *89*, 1861. (b) Henglein, A. *J. Phys. Chem.* **1993**, *97*, 5457. (c) Henglein, A. *Ber. Bunsen-Ges. Phys. Chem.* **1977**, *81*, 556. (d) Henglein, A. *Elektrochemie der Metalle* DECHEMA Monogr. **1983**, *93*, 163.

(27) (a) Sun, S.; Murray, C. B. *J. Appl. Phys.* **1999**, *85*, 4325. (a) Murray, C. B.; Sun, S.; Doyle, H., Betley, T. *MRS Bull.* **2001**, *26*, 985.

(28) (a) Henglein, A.; Giersig, M. *J. Phys. Chem. B* **1999**, *103*, 9533. (c) Henglein, A. *Langmuir* **2001**, *17*, 2329. (b) Henglein, A. *Chem. Mater.* **1998**, *10*, 444.

(29) Talapin, D. V.; Koeppe, R.; Gotzinger, S.; Kornowski, A.; Lupton, J. M.; Rogach, A. L.; Benson, O.; Feldmann, J.; Weller, H. *Nano Lett.* **2003**, *3*, 1677.

(30) (a) Hu, J. Q.; Li, Q.; Wong, N. B.; Lee, C. S.; Lee, S. T. *Chem. Mater.* **2002**, *14*, 1216. (b) Hum J. Q.; Li, Q.; Meng, X. M.; Lee, C. S.; Lee, S. T. *Chem. Mater.* **2003**, *15*, 305.

(31) Mahamuni, S.; Borgohain, K.; Bendre, B. S.; Leppert, V. J.; Risbud, S. H. *J. Appl. Phys.* **1999**, *85*, 2861.

(32) (a) Guo, L.; Yang, S.; Yang, C.; Yu, P.; Wang, J.; Ge, W.; Wong, K. L. *Chem. Mater.* **2000**, *12*, 2268. (b) Guo, L.; Yang, S.; Yang, C.; Yu, P.; Wang, J.; Ge, W.; Wong, G. K. L. *Appl. Phys. Lett.* **2000**, *76*, 2901. (c) Yang, C. L.; Wang, J. N.; Ge, W. K.; Guo, L.; Yang, S. H.; Shen, D. Z. *J. Appl. Phys.* **2001**, *90*, 4489.